Supporting information

Johanna Beckmann[1] and Ricarda Winkelmann[1,2]

[1]Potsdam Institute for Climate Impact Research, RD1, Potsdam, 14473, Germany,
[2]Institute of Physics and Astronomy, University of Potsdam, Potsdam, Germany

Correspondence: Johanna Beckmann (beckmann@pik-potsdam.de)

1 Initial state and comparison to present day

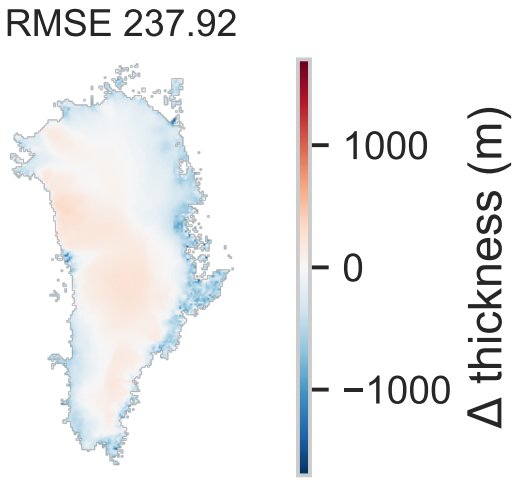

Fig. S1. Thickness anomalies between modelled initial state and observations. Given are the ice thickness differences between observations and the modelled initial state after a glacial cycle, with a RMSE of 237.92 metres. Note that only fields with thicknesses above 1m were taken into account, as this was the original minimum thickness of the BedMachine data Morlighem et al. (2017).

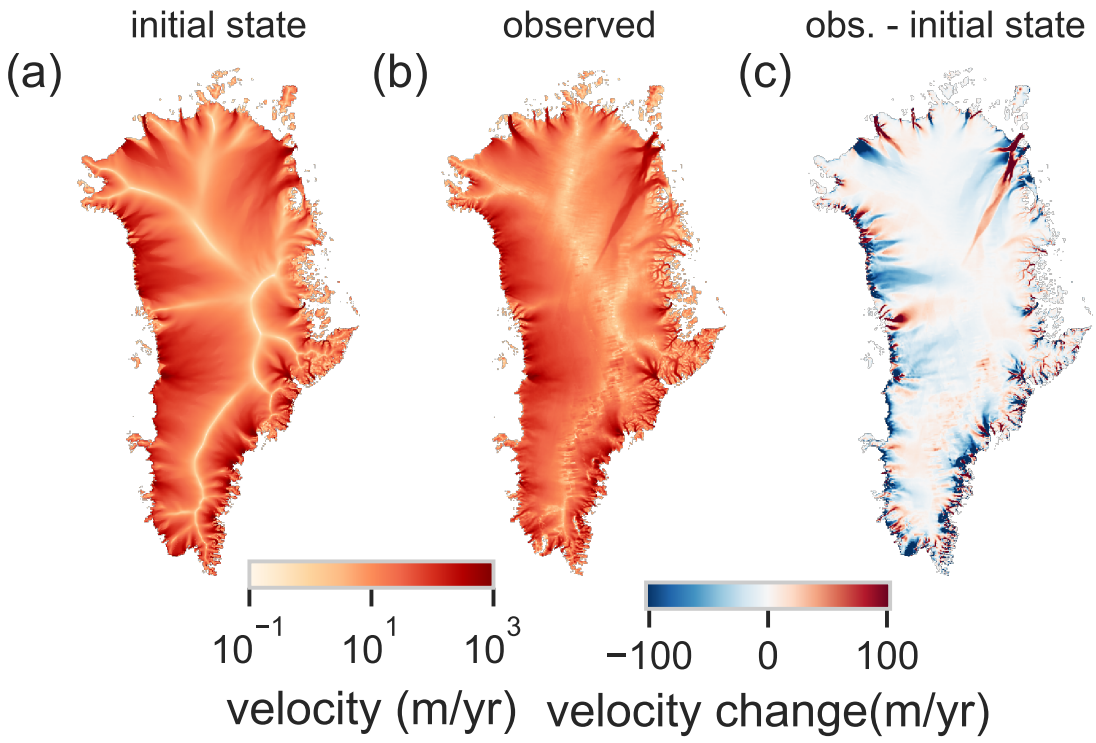

Fig. S2. Ice velocities. a Velocities of initial state and **b** the observed values Joughin et al. (2018), averaged over years 1995-2015. **c** Differences between initial state and observations, with a RMSE of 146 m/yr. Note that only velocity fields with thicknesses above 1m were taken into account, as this was the original minimum thickness of the BedMachine data Morlighem et al. (2017)

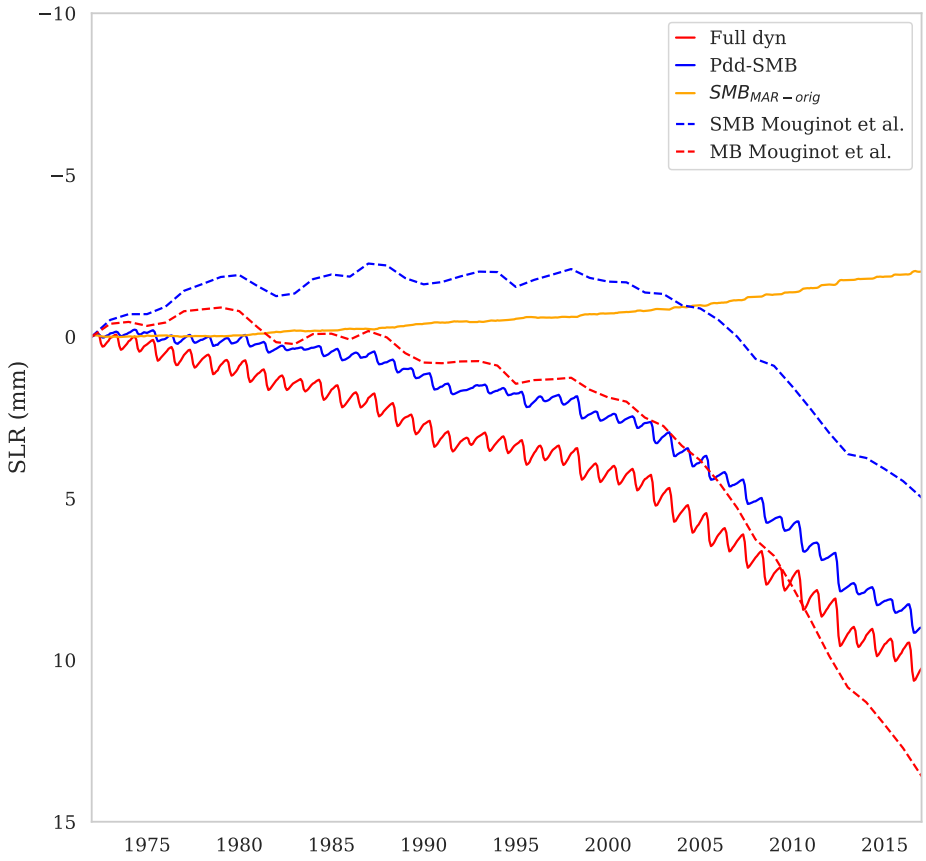

Fig. S3. Historical simulation(1972-2017) and observations. Given are the calculated SLR from PISM simulations full dynamic run in red and the cumulative SMB changes form the climatological mean from 1971-1999 calculated by the PISM-PDD model (blue) forced with the ERA-Temperature from 1972-2017. The full dynamic runs is subtracted by the control run (Fig. S15,SI). Observation Mouginot et al. (2019) from the cumulative SMB loss (blue dashed) were calculated by cumulative SMB anomalies of the SMB mean from 1961-1989. The cumulative mass balance is depicted with the red dashed line. The cumulative SMB changes of climatological mean of 1971-1999 from the original MAR data give a sea level rise equivalent depicted in with the orange line.

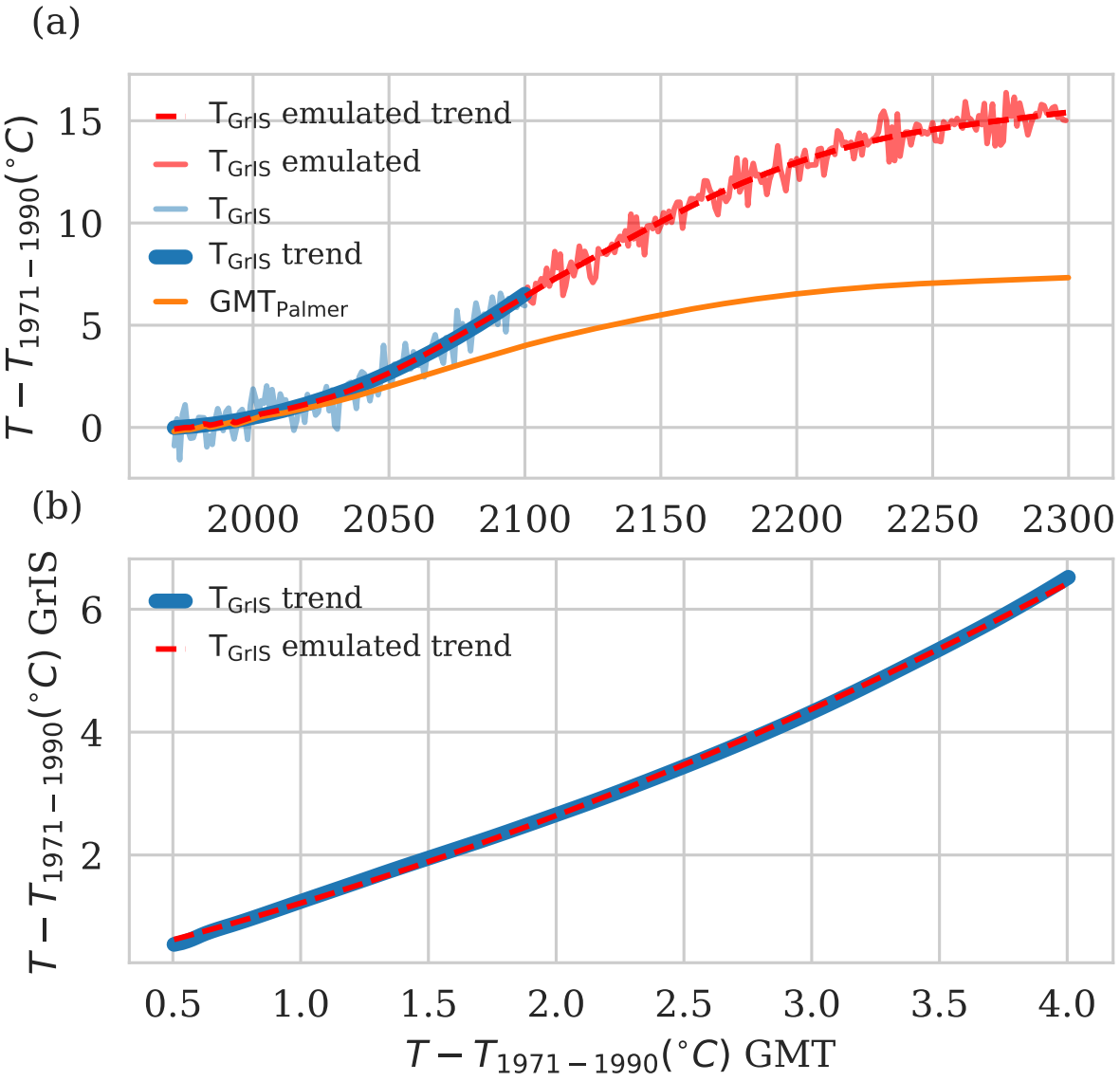

Fig. S4. Emulation of the annual average temperature anomaly over Greenland from 2100 to 2300. a Given is the emulated annual average temperature anomaly of Greenland (T_{GrIS} emulated; red solid line) and its trend (T_{GrIS} emulated trend; red dashed line) from 2100 until 2300, the annual temperature anomaly from MAR-Miroc5 (T_{GrIS}, blue solid line) and its derived quadratic trend (T_{GrIS} trend$= 1280.16^{\circ}C - 1.31^{\circ}C/year \cdot years + 20^{\circ}C/year^{-2} \cdot years^2$, blue thick line) from 1971 until 2100 as well as the global mean temperature from 1971 until 2300 emulated by Palmer et al. Palmer et al. (2018) (orange line). **b** The temperature trend (T_{GrIS} trend, blue thick line) until 2100 and the global mean temperature until 2100 was used to derive an emulation function for the T_{GrIS} in dependence of the global mean temperature (GMT) with T_{GrIS} emulated trend$= 0.1^{\circ}C + 0.96^{\circ}C^{-1} \cdot GMT + 0.15^{\circ}C^{-2} \cdot GMT^2$ (red dashed line). This emulation function was then used to derive the emulated trend until year 2300 shown in **a**.

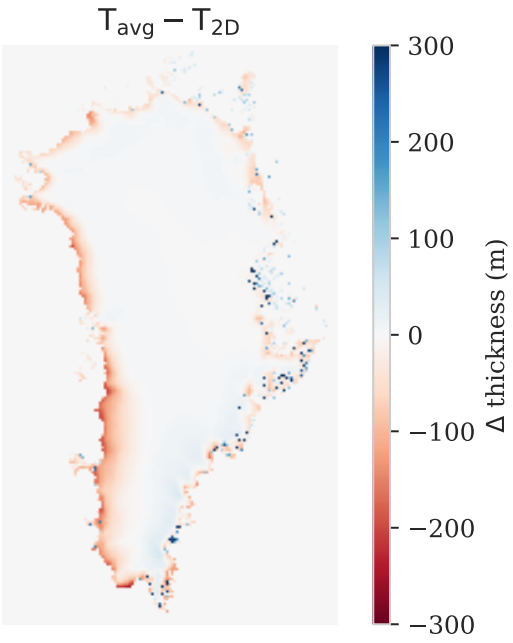

Fig. S5. Difference of ice thickness with pdd-simulations using a scalar temperature field and a spatial 2D temperature field at the year 2100. The reddish area shows where our ice loss simulation is overestimated compared to simulations with a 2D temperature field in the year 2100. Blueish area show the regions of underestimated mass loss.

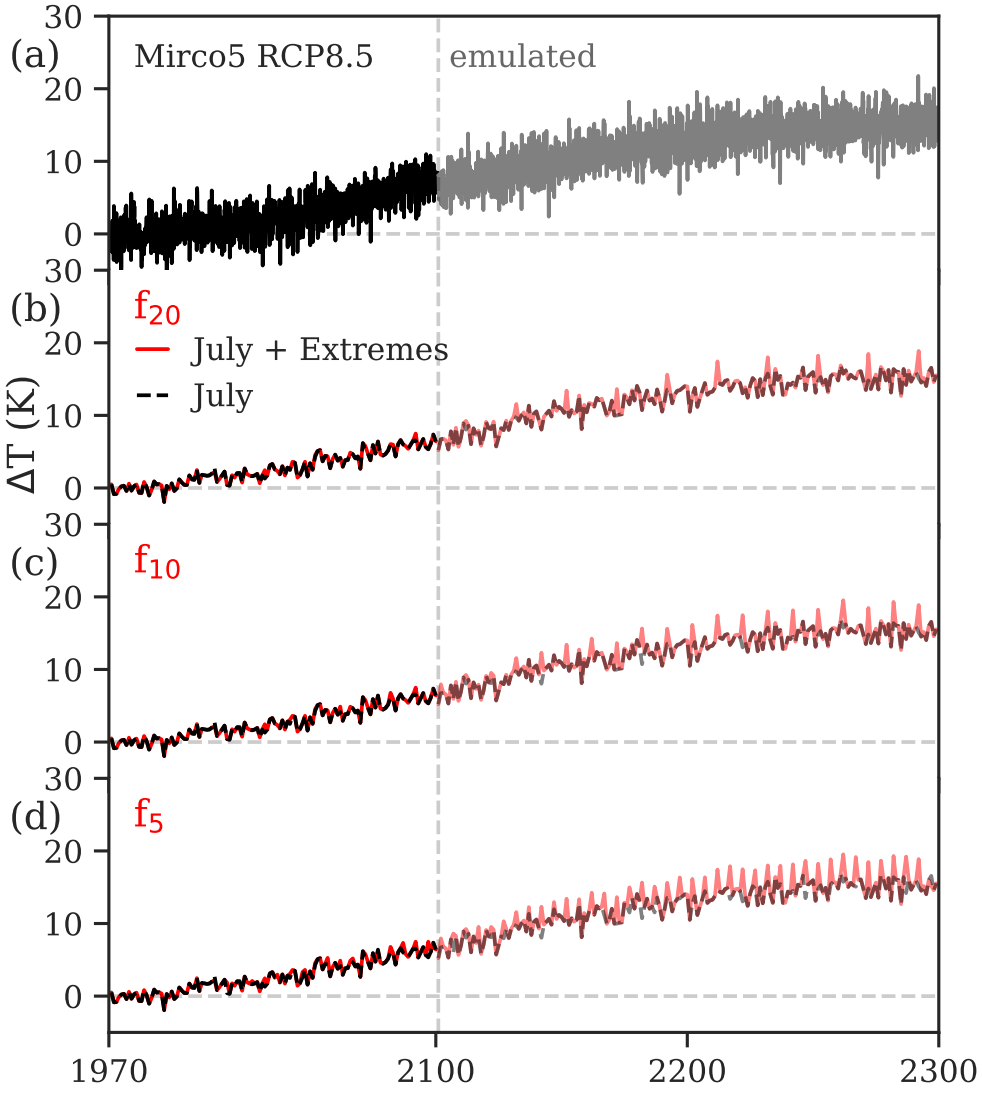

Fig. S6. Temperature scenarios $I_{1.25}$ for the Greenland Ice Sheet. Given is the temperature anomaly over Greenland, based on the MIROC5 RCP8.5 projections, which is applied uniformly at the ice-sheet surface. **a** The forcing scenario without extremes on a monthly timescale (black, solid) from Miroc 5 projection until year 2100, and emulated (grey) thereafter (see Methods). **b-d** July temperature projection (black, dashed) including extremes (red) occurring every 20 (f_{20}), 10 (f_{10}) and 5 (f_5) years with an intensity of 1.25 times the 10-year running mean ($I_{1.25}$).

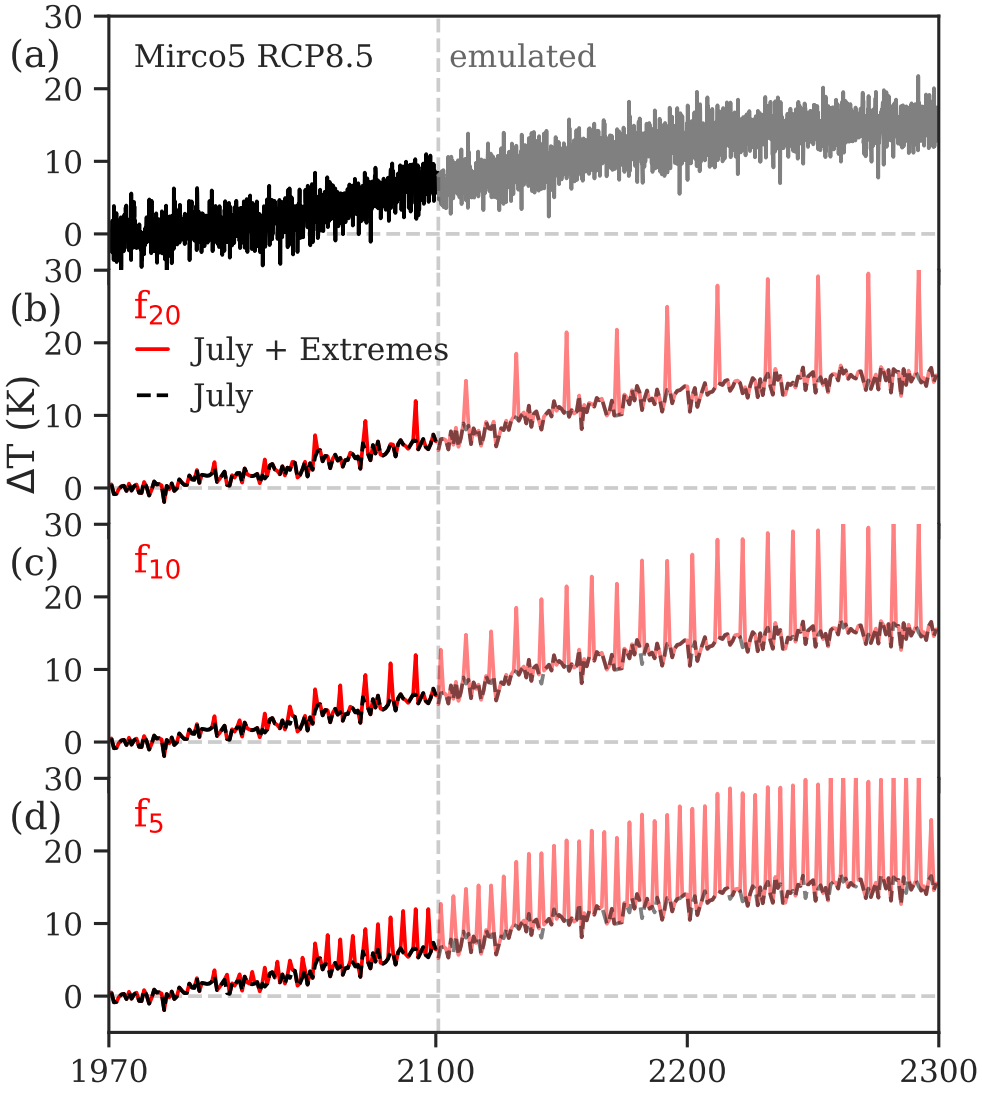

Fig. S7. Temperature scenarios I_2 for the Greenland Ice Sheet. Given is the temperature anomaly over Greenland, based on the MIROC5 RCP8.5 projections, which is applied uniformly at the ice-sheet surface. **a** The forcing scenario without extremes on a monthly timescale (black, solid) from Miroc 5 projection until year 2100, and emulated (grey) thereafter (see Methods). **b-d** July temperature projection (black, dashed) including extremes (red) occurring every 20 (f_{20}), 10 (f_{10}) and 5 (f_5) years with an intensity of 2 times the 10-year running mean (I_2).

2.1 Evolution of extremes

Based on our knowledge of the past temperature distribution including the respective frequencies of extremes ($\mathrm{f_{old}}$) and temperature levels reached during an extreme event ($\mathrm{T_{old}}$)), we can put future extremes occurring in generally warmer climates into context:

The temperature distribution can either shift to higher temperatures or the variance can broaden or the combination of the two might happen. All three cases lead to a higher frequency of the extreme temperatures observed in the old climate $\mathrm{f_{new}(T_{old})}$. Similarly this means that the extreme frequency of the old climate are now substituted by higher temperatures $\mathrm{f_{old}(T_{new})}$. How much these new extreme temperatures might actually increase in future we can only speculate, but it is certain that with increased temperatures the intensity of the extremes will get higher, as the distribution shifts or broadens more and more. For simplicity, we therefore here use idealized scenarios, applying a factor of 1.25, 1.5 and 2 times to the 10-year running mean. Note that in our approach the 10-year running mean always refers to the baseline scenario and excludes potentially added extremes from the years before. Figures S5 and S6 show that the extremes would increase in a similar manner if we calculated them from the observed temperature distributions and standard deviation of the past years. For example, the 2012 July temperature was 2.6 standard deviations above the 1971-2011 mean. Considering new extremes with the same 2012-deviation, leads to a temperature increase comparable to our $\mathrm{I_{1.5}, f_5}$ scenario (Fig. SS8). Similarly does this approach compare well with our $\mathrm{I_2, f_5}$ scenario if the temperature distribution of only the last 15 years is considered (Fig. SS9). Note that in this case, every new extreme adds to the temperature distribution thereafter.

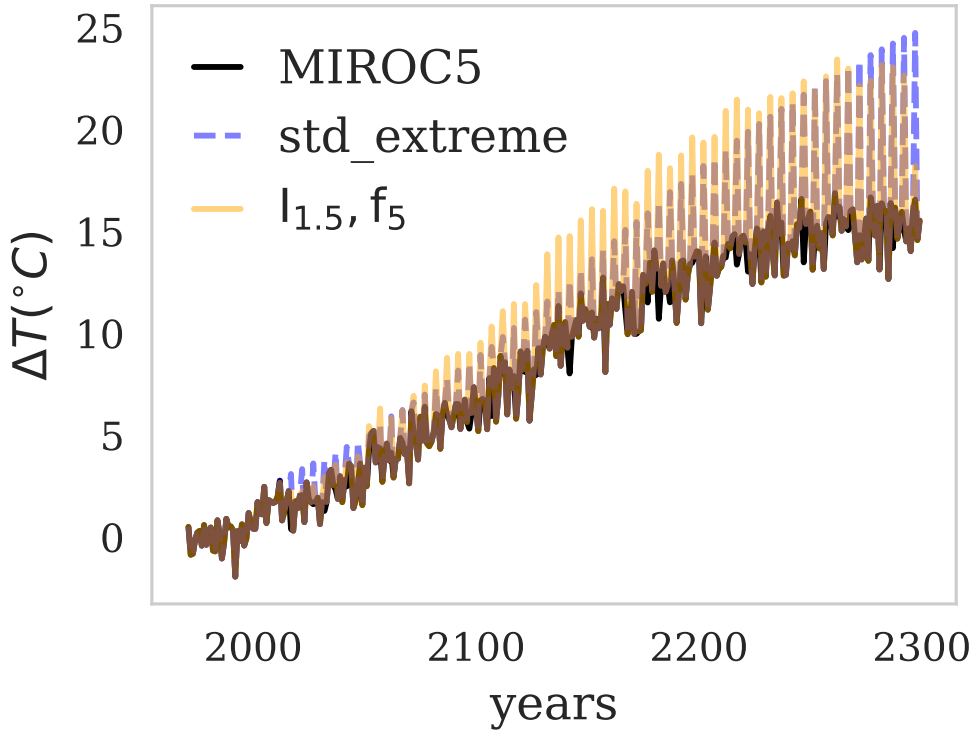

Fig. S8. Evolution of different extreme temperature scenarios from past temperature distribution. Given is the temperature anomaly over Greenland, based on the MIROC5 RCP8.5 projections (black) and the scenarios$I_1.5, f_5$ (yellow). Looking at the July temperature distribution from 1979 until 2011, the 2012 temperature was 2.6 standard deviations from the mean value away. Every 5 years the new extreme is created by looking at the past temperature distribution from 1979 to the current year and adding a extreme temperature that is 2.6 standard deviations away from the total mean (blue dashed). Subsequent extreme calculations includes a temperature distribution that contains bygone extremes.

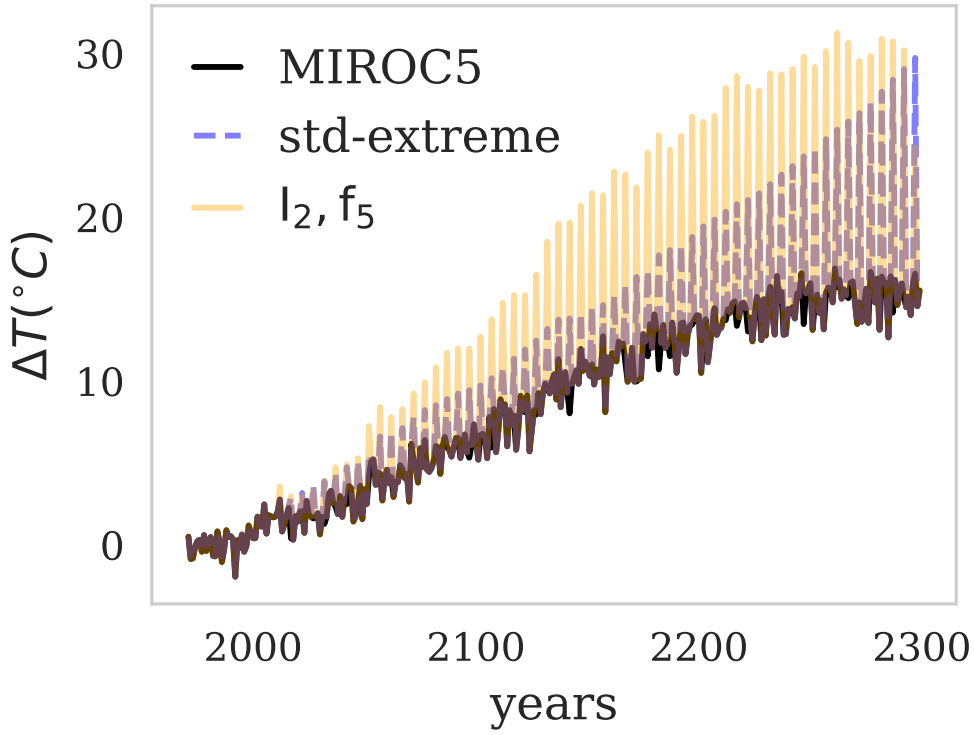

Fig. S9. Evolution of different extreme temperature scenario from 15-year temperature distribution . Given is the temperature anomaly over Greenland, based on the MIROC5 RCP8.5 projections (black) and the scenariosI_2, f_5 (yellow). Using the the last 15-years of July temperature gives that the 2012 extreme event was 2.2 standard deviation of the 1996-2011 histogram . Adding every 5 years an extreme with the same standard deviation of its past 15-year temperature distribution (thus including newly created extremes) leads to the blue dashed line.

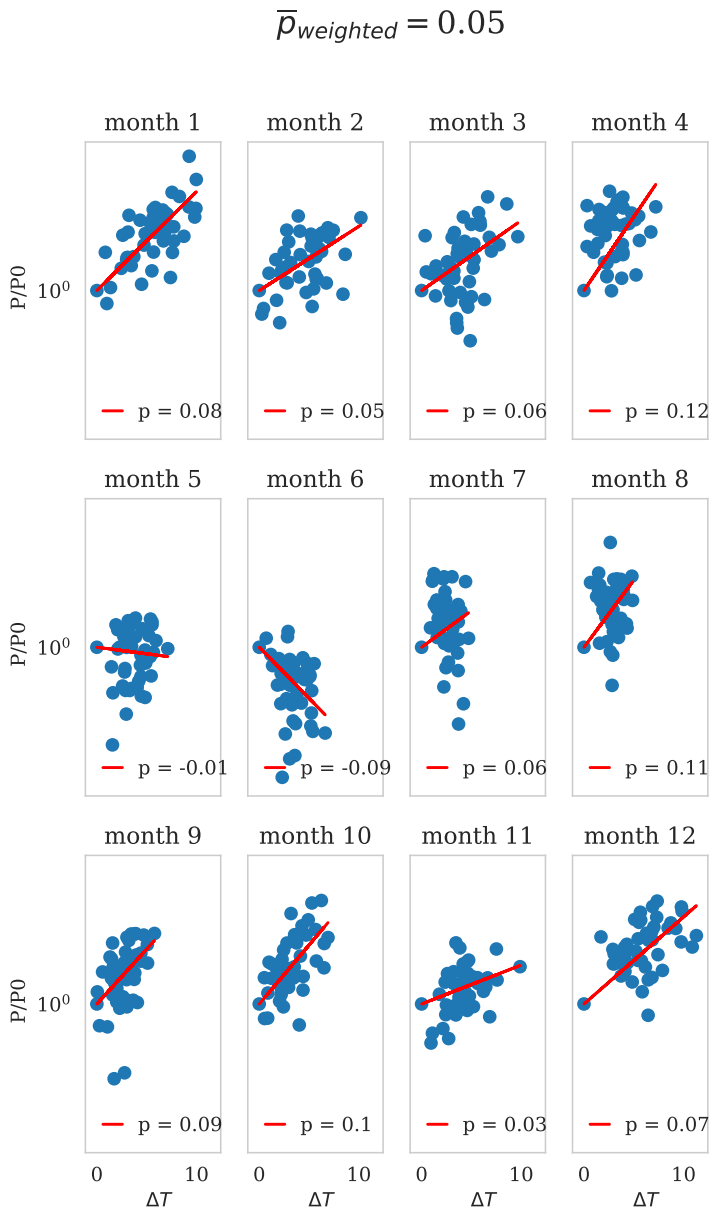

Fig. S10. Determination of precipitation factor p for the precipitation function $P = P_0 exp(p \cdot \Delta T)$ for the ERA Interim dataset. Each panel shows the monthly difference of precipitation P and the minimum precipitation at this month P_0 in 1971-2015 on a logarithmic scale and the temperature difference of $P - P_0$ (blue dots).The red line gives the determined monthly precipitation factor p. As a weighted sum they define the universal precipitation increase of 5% per degree of warming used in the experiments.

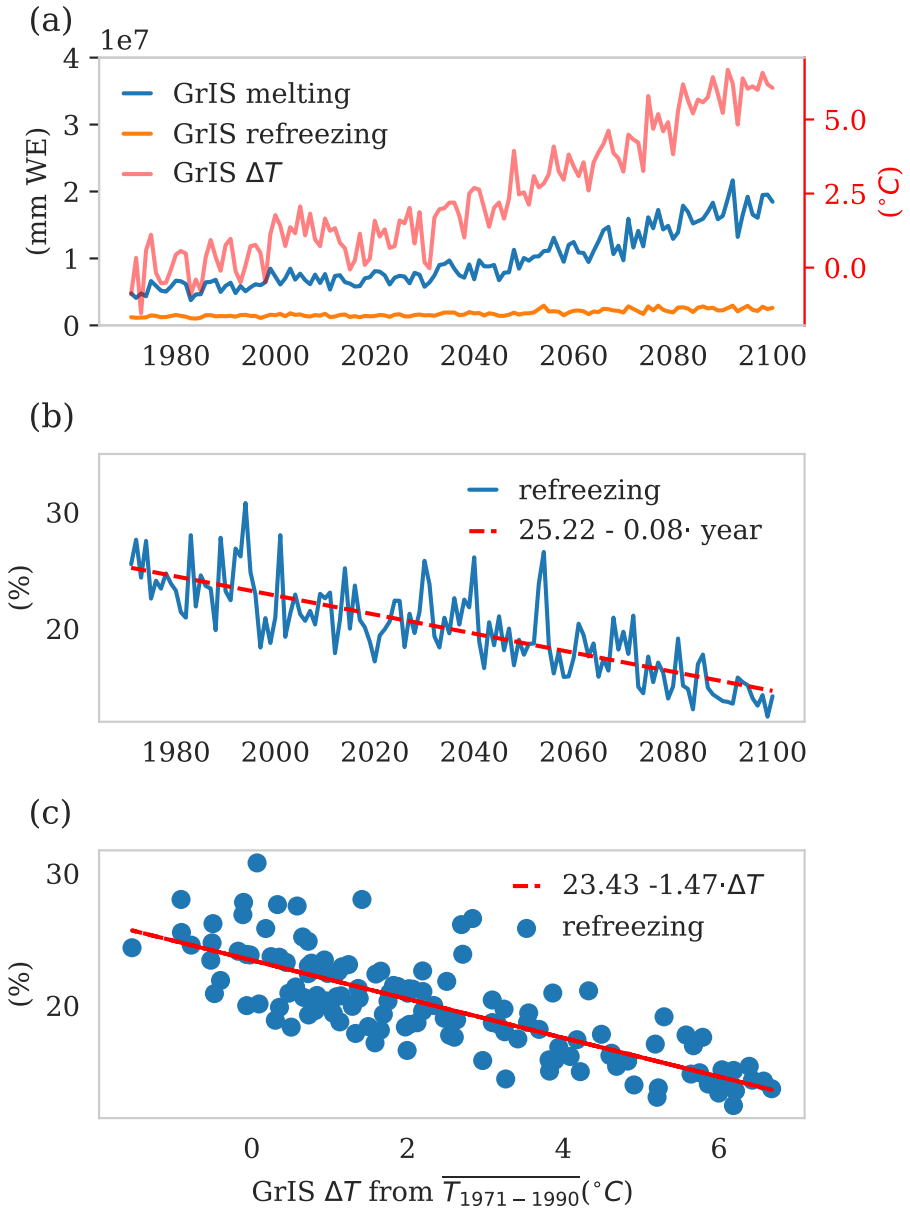

Fig. S11. Determination of refreezing parameter from the average surface temperature anomaly in Greenland. **a** Shown are the total melting (blue line), refreezing (orange line) and temperature over Greenland (reddish shading) over time, **b** the percentage of refreezing over time (blue line). The trend in time is given by $25\% - 0.05\%/year$ (red dashed line). **c** The temperature-dependent refreezing (blue points) determined with the percentage refreezing in **b** and the temperature anomaly in **a**. The red dashed line gives the temperature-dependent percentage refreezing function $(23.42 - 1.35 \cdot \Delta T)$.

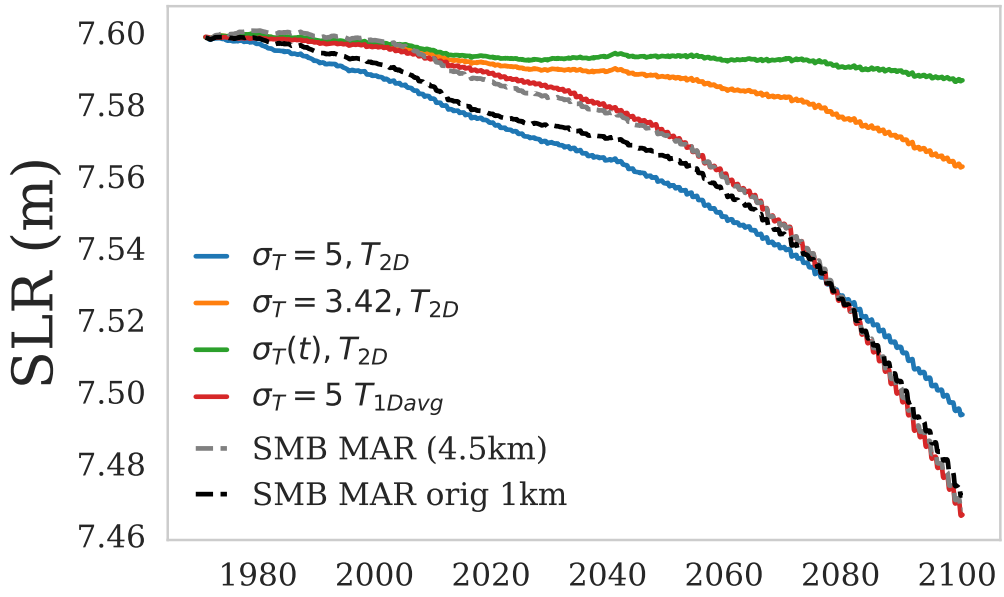

Fig. S12. Sea-level rise for different PDD parameters. Shown is the SLR calculated from a SMB-only scenario (without subtraction of the control run) with the temperature-dependent refreezing function determined in Fig. S11 for different constant standard deviations of 5 and 3.42, and a time-dependent temperature standard deviation $\sigma(t)$ derived from the Miroc5 data set. SLR from the original MAR data set (Miroc5) of 1km resolution was derived from the ΔSMB while the SLR projection on 4.5 km resolution was recalculated considering only mass loss from ice thickness above flotation.

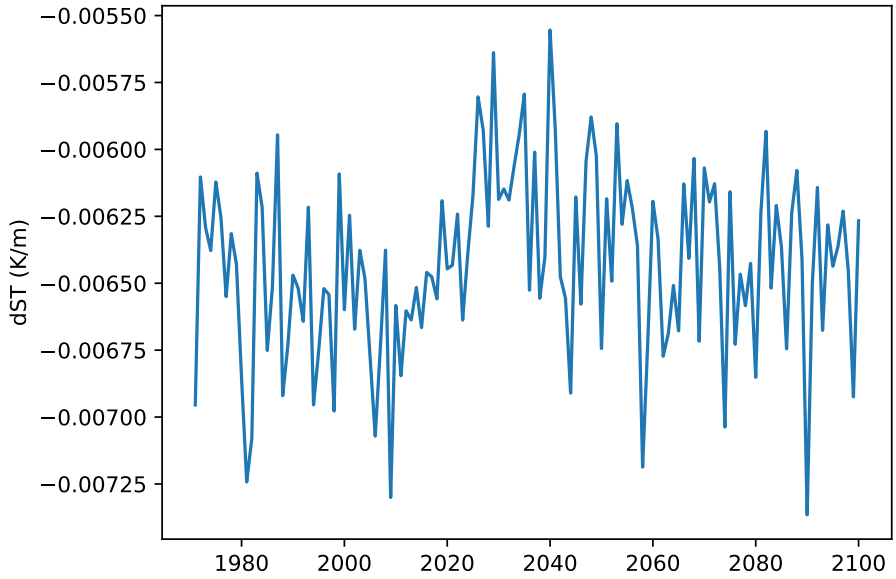

Fig. S13. Surface temperature gradient averaged over the GrIS. Temperature gradient was taken form the yearly MAR data sets for ERA and MIROC5.

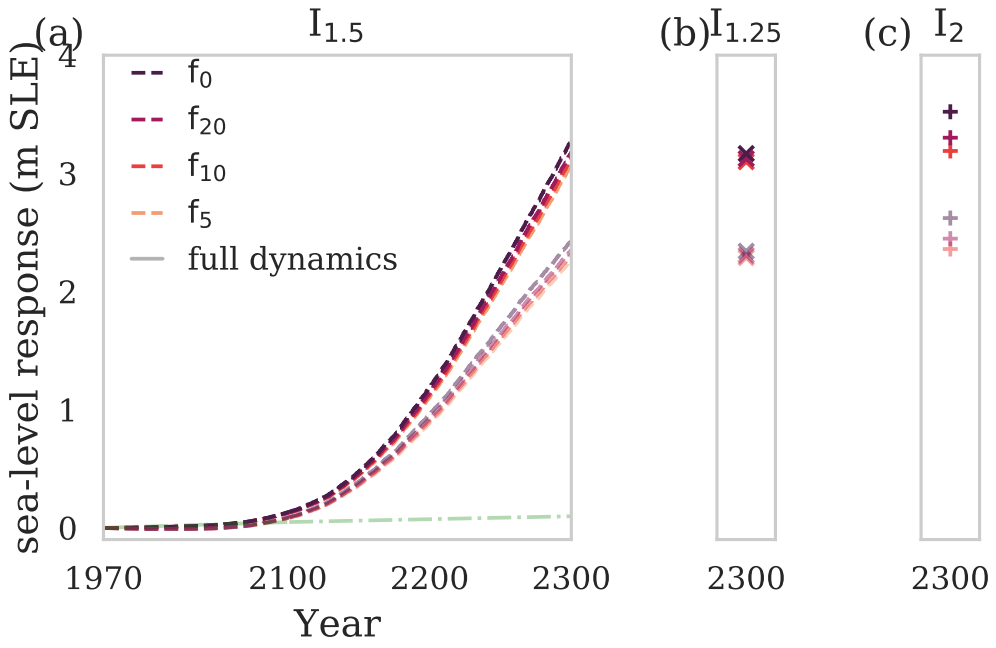

Fig. S14. Sea-level rise contribution of the Greenland Ice Sheet until 2300. **a** Fully dynamic sea-level rise contribution (dark colors) until 2300 for the forcing scenario without extremes (orange) and the extremes scenarios f_{20} (red), f_{10} (pink) and f_5 (purple) with intensity $I_{1.5}$. Light colors indicated the sea-level change due to SMB changes only.All run are subtracted by the control run (light green). The corresponding ice sheet extent in 1971 (i) and the emerging ice retreat in years 2100 (ii), 2200 (iii) and 2300 (iv) are given in light blue and red shading, respectively. **b,c** Sea level rise contribution for the same experiments but for lower and higher extreme event intensities of $I_{1.25}$ and I_5, respectively.

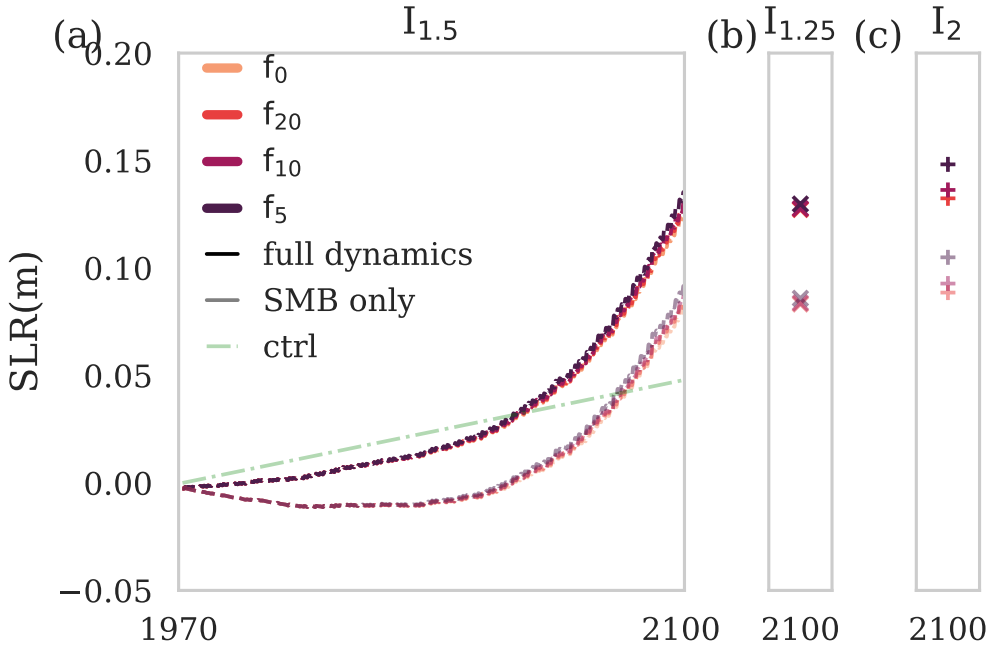

Fig. S15. Sea-level rise contribution of the Greenland Ice Sheet until 2100. **a** Fully dynamic sea-level rise contribution (dark colors) until 2300 for the forcing scenario without extremes (orange) and the extremes scenarios f_{20} (red), f_{10} (pink) and f_5 (purple) with intensity $I_{1.5}$. Light colors indicated the sea-level change due to SMB changes only.All run are subtracted by the control run (light green). **b,c** Sea level rise contribution for the same experiments but for lower and higher extreme event intensities of $I_{1.25}$ and I_5, respectively.

ΔT	$\Delta\text{SMB}_{\text{MIROC5}}$ (Gt yr^{-1})	$\Delta\text{SMB}_{\text{I}_2,\text{f}_5}$ (Gt yr^{-1})	$\Delta\text{SMB}_{\text{I}_2,\text{f}_5}/\Delta\text{SMB}_{\text{MIROC5}}$
0K	0.0	0.0	-
1.5K	-123.0	-147.0	1.2
2K	-165.0	-199.0	1.2

Table 1. Mean GrIS-integrated anomalies of annual SMB (Gt yr^{-1}) **compared to 1980–1999.** Given are the means for the baseline scenario and our most severe extreme scenario(I_2, f_5) as well as the relative SMB increase between the two.

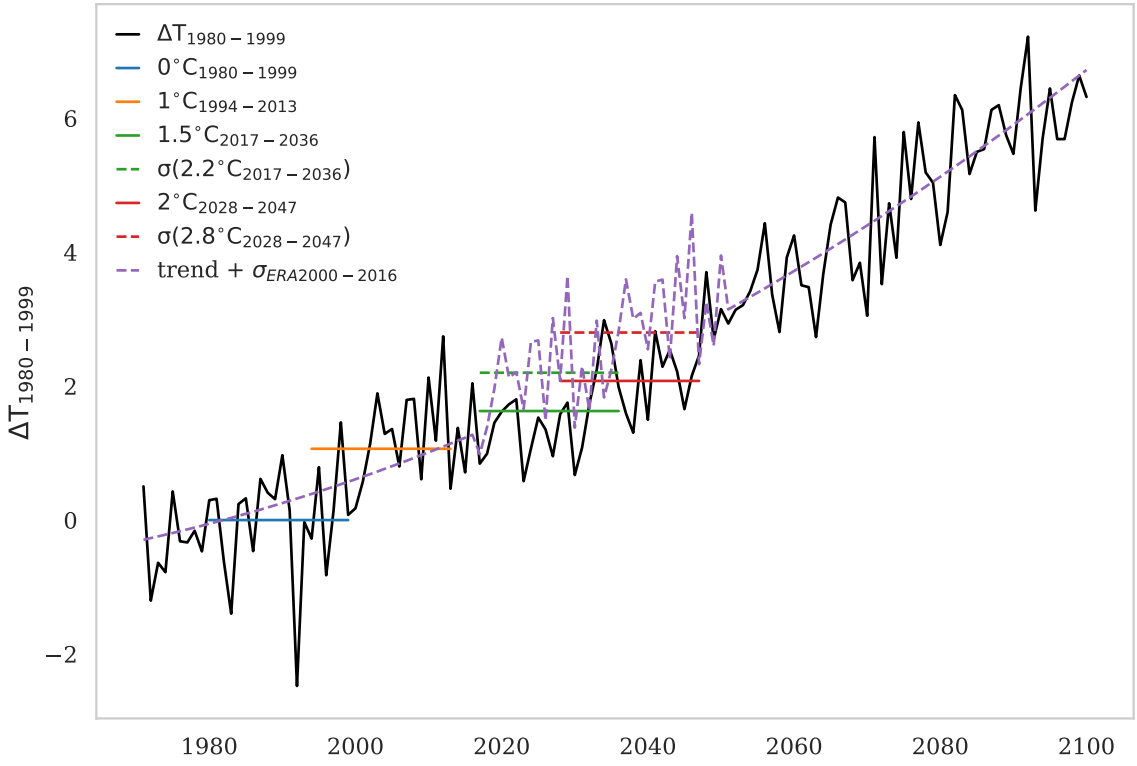

Fig. S16. Summer Temperature anomalies to the mean of 1980-1999. Given is the summer (June-July-August) temperature anomaly to the mean of 1980-1999 in order to compare with Delhasse et al.Delhasse et al. (2018). The solid colored lines give the time frame in which a mean temperature increase of 1K (1994-2014, orange), 1.5K (2017-2037, green) and 2K (2028-2048, red) is achieved with our temperature curve of the base line scenario(ERA until 2017 and MIROC5 after 2017). The purple dashed line depicts the trend of our baseline scenario plus the de-trended variability from 2000-2016 added for the time 2017- 2051. The mean temperature of the same time frames as of the baseline scenario is depicted with the colored dashed lines: 2.2K (2017-2037, green dashed) and 2.8K (2028-2048, red dashed)

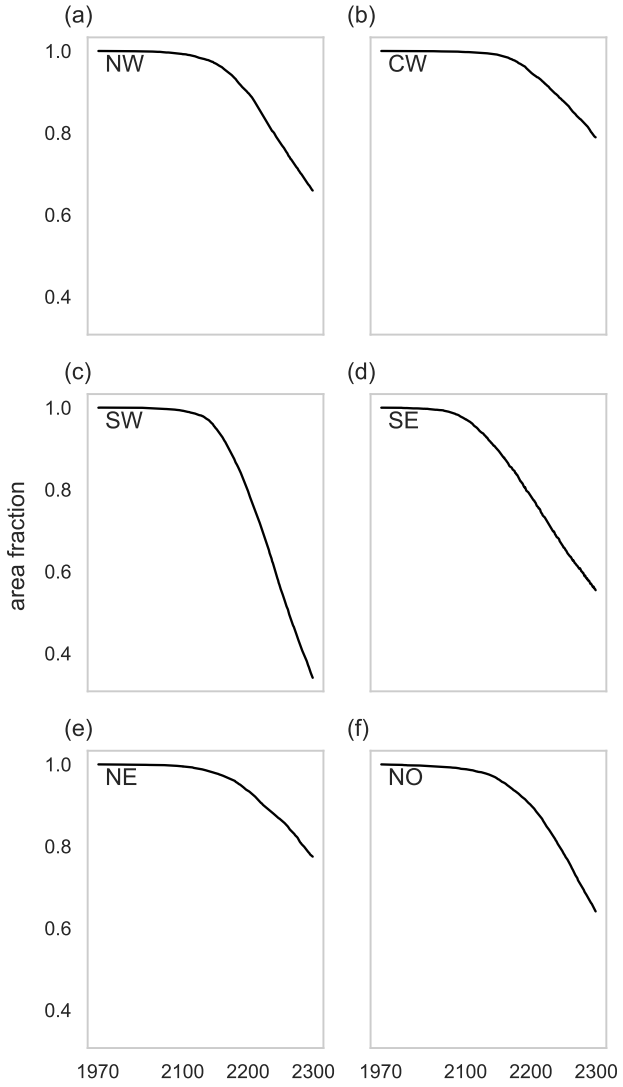

Fig. S17. Area fraction covered by the ice sheet $I_{1.5}, f_5$. Each panel shows the relative area covered by the ice sheet in respect to the year 1970 for each sector.

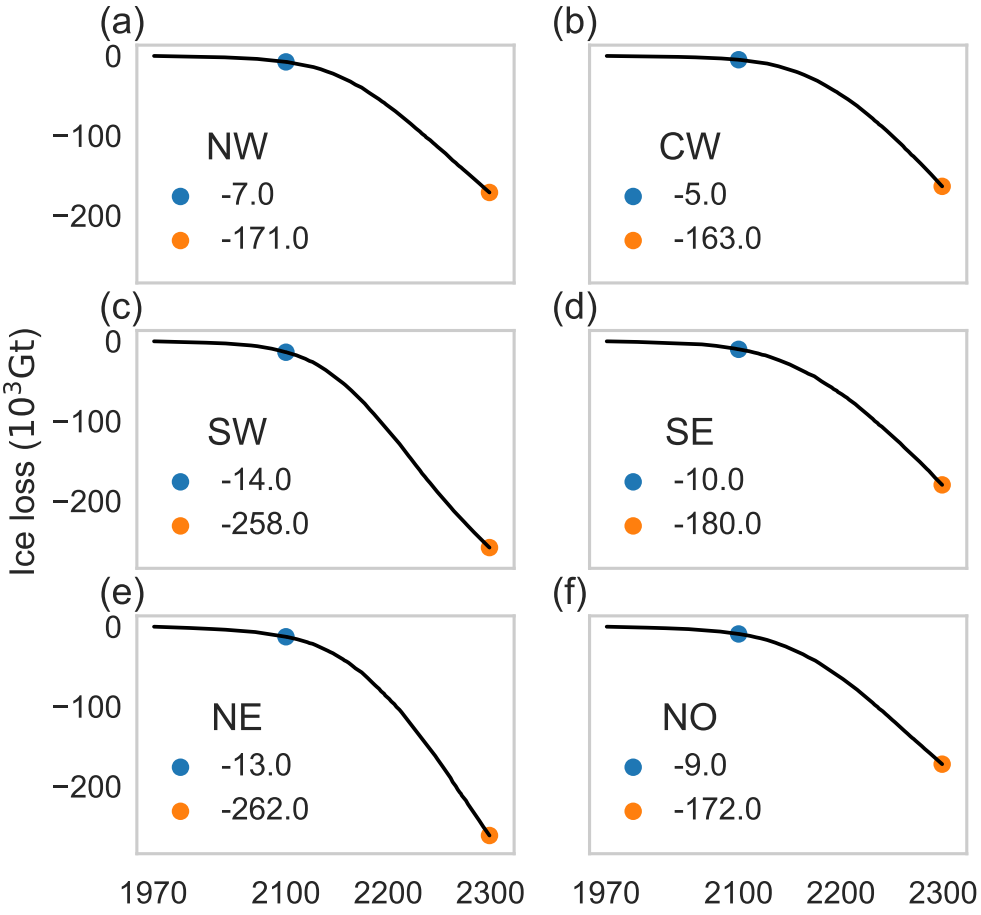

Fig. S18. Absolute ice loss from original ice volume for each sector for $I_{1.5}, f_5$. Each panel shows the ice volume changes over time for each sector. Given are the losses in the year 2100 (blue dot) and 2300 (orange dot). Note that only fields with thicknesses above 1m were taken into account, as this was the original minimum thickness of the BedMachine data Morlighem et al. (2017).

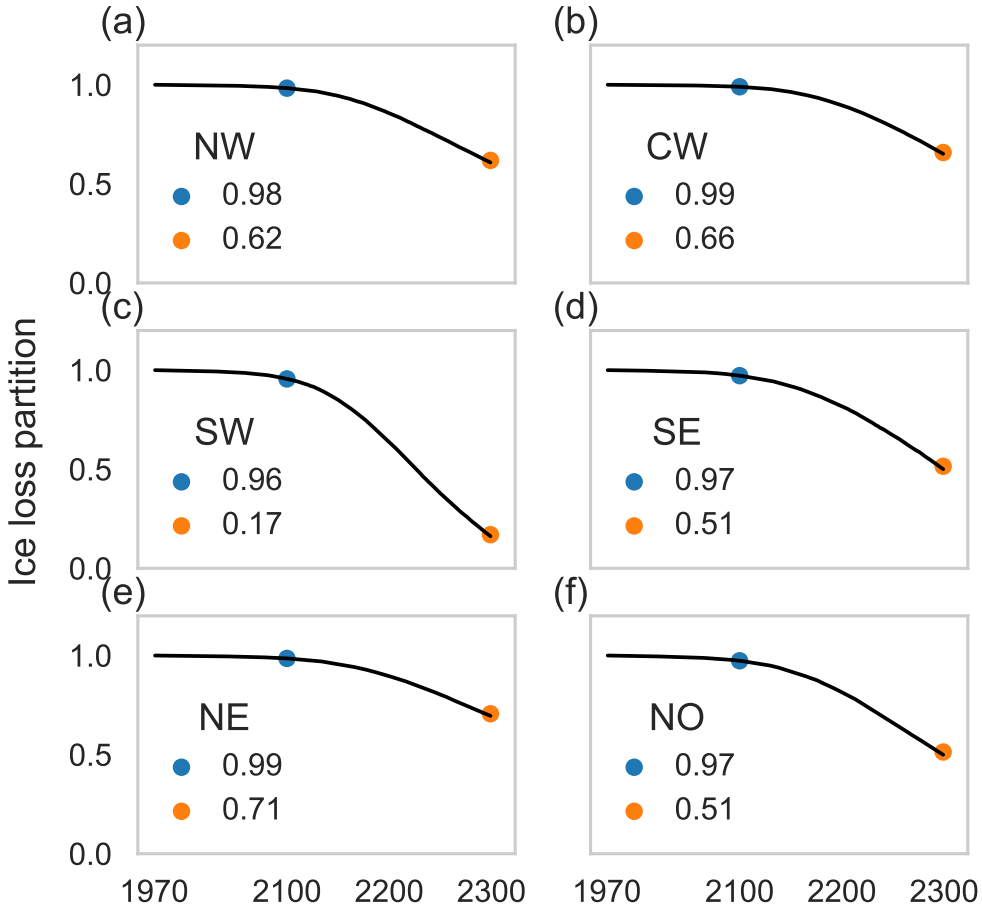

Fig. S19. Relative ice loss from original ice volume for each sector for $I_{1.5}, f_5$. Each panel shows the ice volume changes over time divided by its original ice volume in year 1970 for each sector. Given are the losses in the year 2100 (blue dot) and 2300 (orange dot). Note that only fields with thicknesses above 1m were taken into account, as this was the original minimum thickness of the BedMachine data Morlighem et al. (2017).

$I \backslash f$	Miroc5 (f=0)	f_{20}	f_{10}	f_5
1.25	297.57	298.51	300.00	301.95
1.50	297.57	300.10	302.62	306.42
2.00	297.57	302.72	306.91	317.22

Table 2. Ice area loss in 2300. Given is the ice area loss in $10^3 \mathrm{km}^2$ for all intensity scenarios (I) and frequency ranges (f). The initial total ice volume covered an area of 2136.86 $10^3 \mathrm{km}^2$.

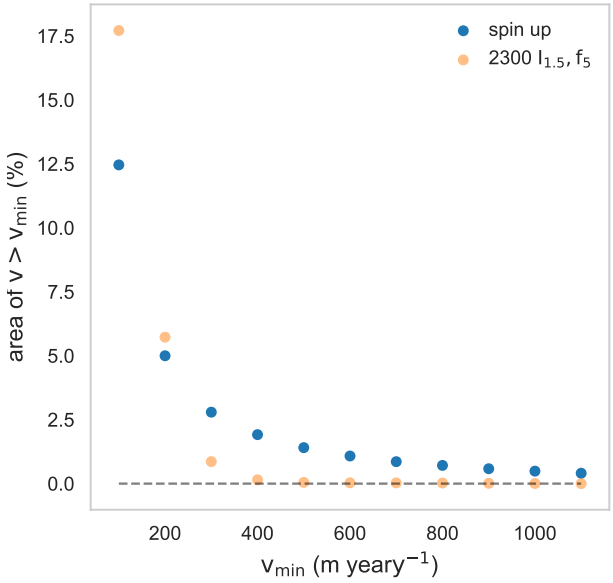

Fig. S20. Area percentage with certain minimum surface velocities. Area fraction is calculated from the ice sheet of the spin-up state (blue) the remaining ice sheet of the year 2300 for the extreme scenario $I_{1.5}, f_5$ in light orange. Note that only fields with thicknesses above 1m were taken into account, as this was the original minimum thickness of the BedMachine data Morlighem et al. (2017).

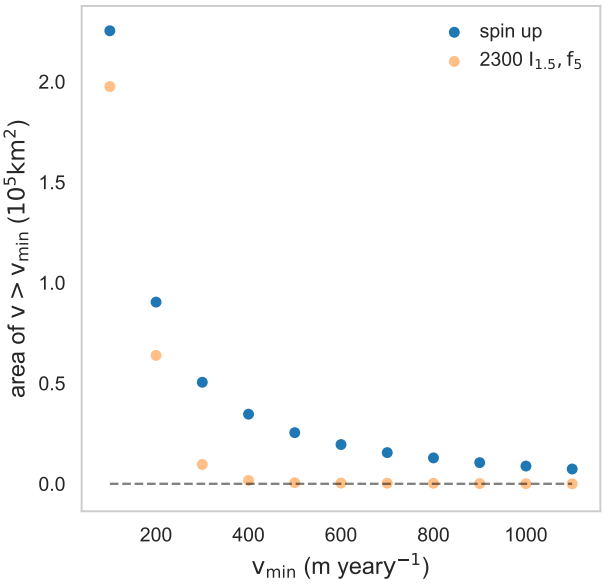

Fig. S21. Area size with certain minimum surface velocities. Area is calculated from the ice sheet of the spin-up state (blue) the remaining ice sheet of the year 2300 for the extreme scenario $I_{1.5}, f_5$ in light orange. Note that only fields with thicknesses above 1m were taken into account, as this was the original minimum thickness of the BedMachine data Morlighem et al. (2017).

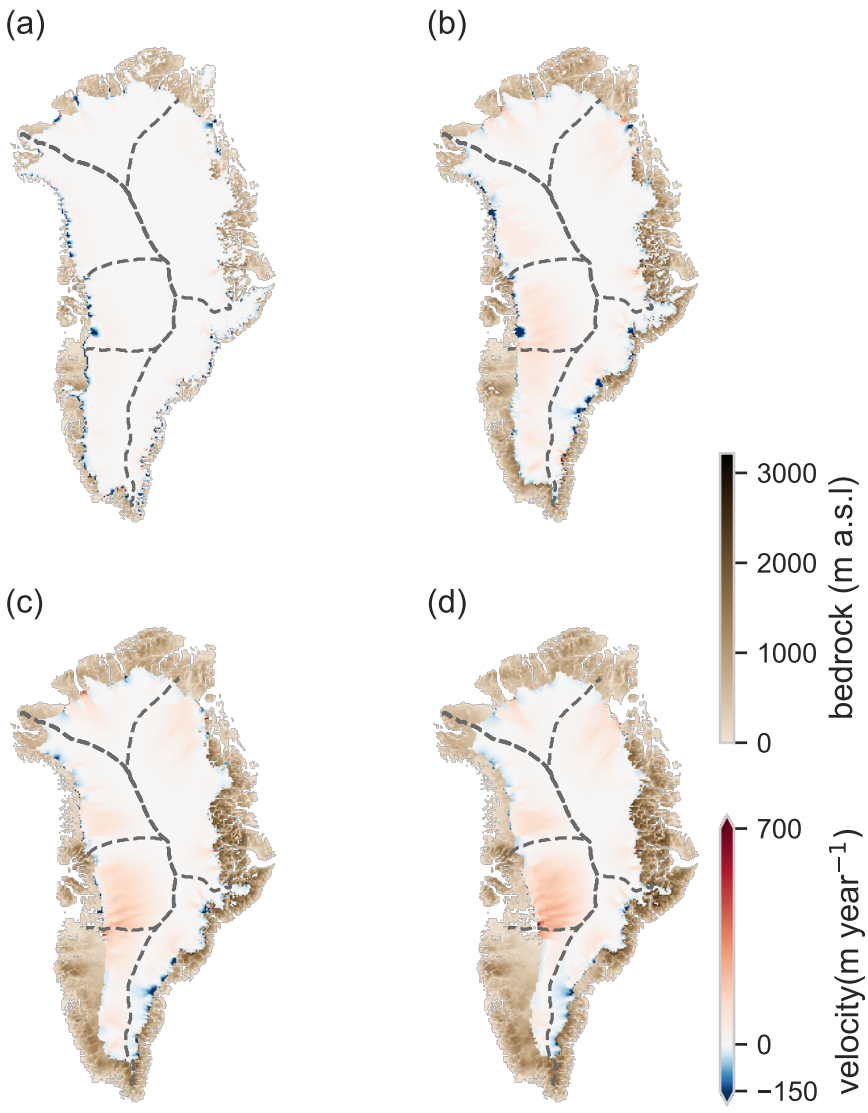

Fig. S22. Surface velocity difference of the $I_{1.5}, f_5$ scenario compared to the spin up velocities. For the remaining ice thickness the surface velocity field is subtracted by the surface velocity field of the spin-up state, for the year a)2100 b)2200 c)2250 and d) 2300 for the $I_{1.5}, f_5$ scenario. Reddish area means speedup while blueish area indicate slow down of the surface ice flow. Note that only fields with thicknesses above 1m were taken into account, as this was the original minimum thickness of the BedMachine data Morlighem et al. (2017).

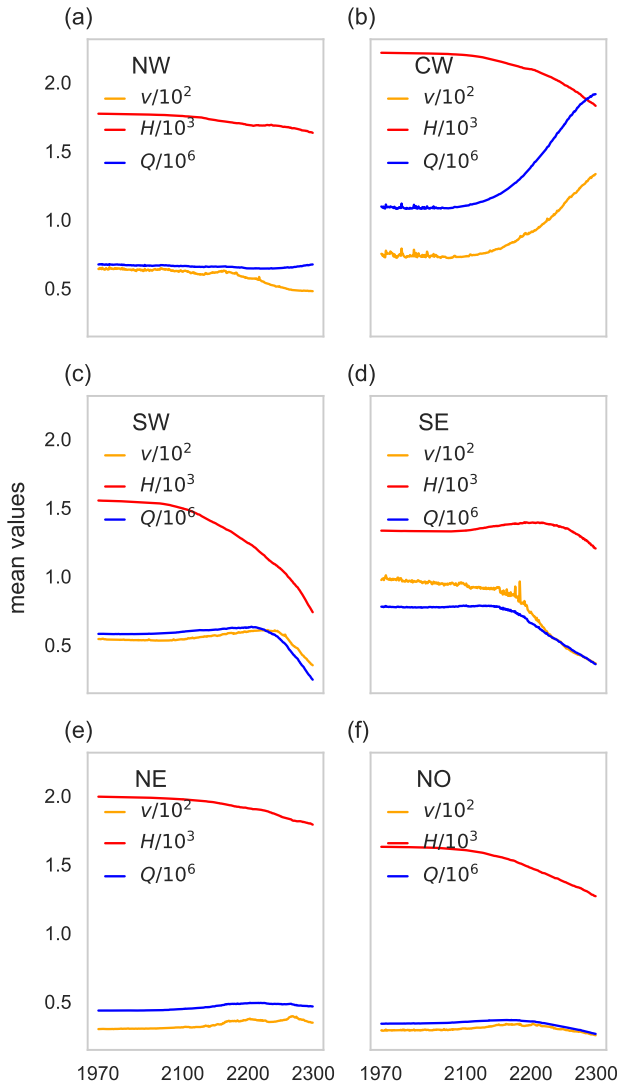

Fig. S23. Mean values of surface velocity (v), thickness (H) and flux (Q) for the $I_{1.5}, f_5$ scenario. Each panel shows the mean values of surface velocity (v in yellow), thickness (H in red) and flux (Q in blue) multiplied by a constant factor of 10^{-2} ,10^{-3} and 10^{-6}/190g respectively for each sector. Note that only fields with thicknesses above 1m were taken into account, as this was the original minimum thickness of the BedMachine data Morlighem et al. (2017).

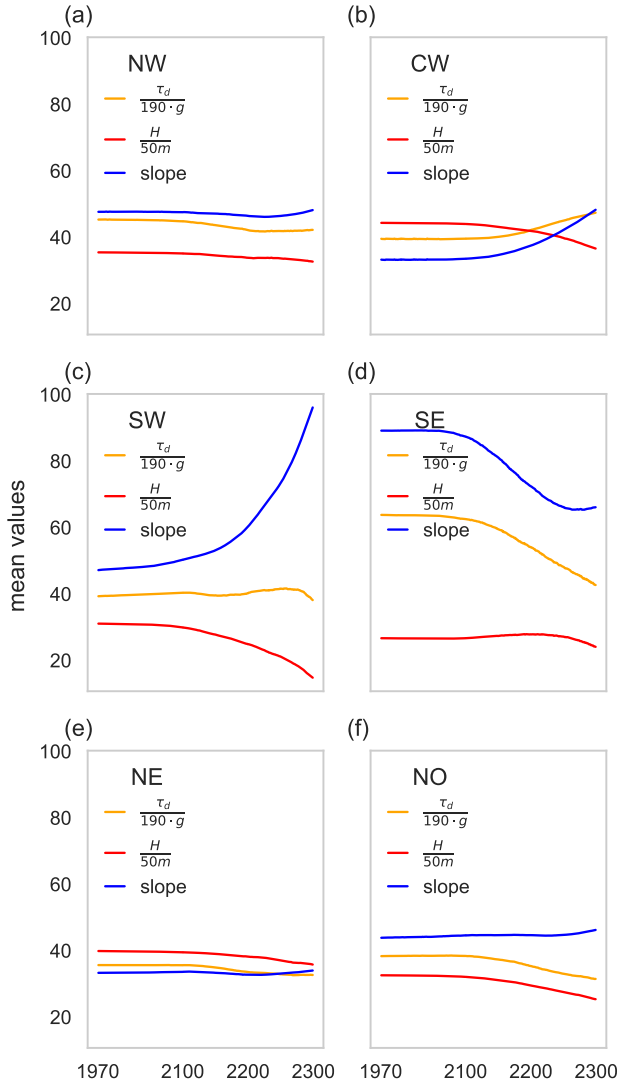

Fig. S24. Mean values of thickness (H), slope and driving stress τ_{d} for the $I_{1.5}, f_5$ scenario. Each panel shows the mean values thickness (H in red), slope in blue and driving stress τ_{d} in yellow multiplied by a constant factor of 1/50 ,1 and /190g respectively for each sector. Note that only fields with thicknesses above 1m were taken into account, as this was the original minimum thickness of the BedMachine data Morlighem et al. (2017)

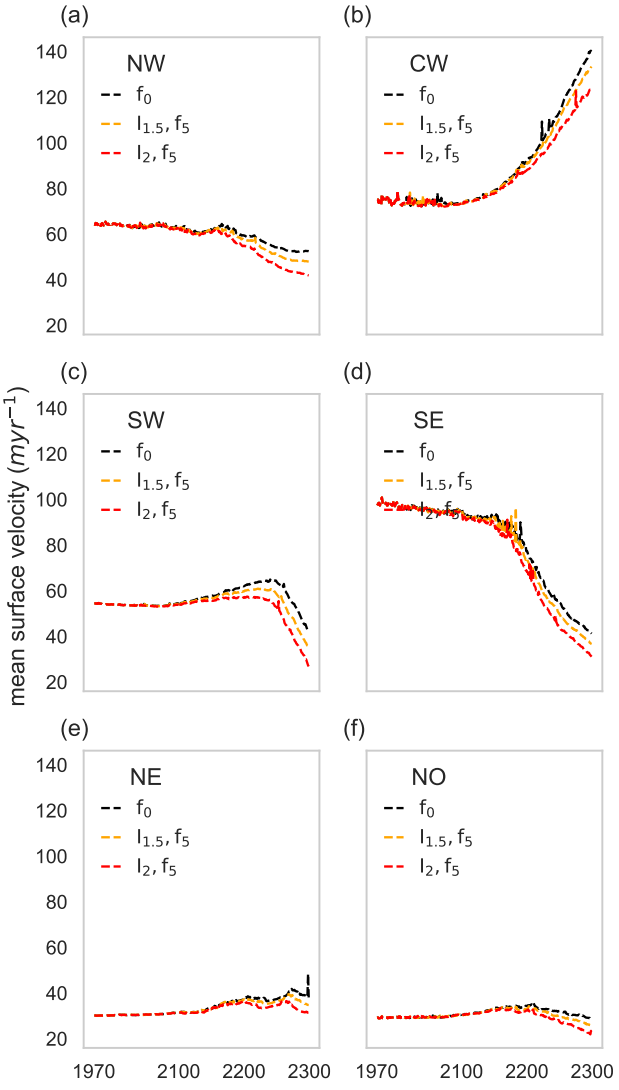

Fig. S25. Mean values of surface velocity for baseline and extreme scenarios .Each panel shows the mean values of surface velocity for the baseline (black), $I_{1.5}, f_5$ (orange) and the $I_{1.5}, f_5$ (red) scenario for each sector. Note that only fields with thicknesses above 1m were taken into account, as this was the original minimum thickness of the BedMachine data Morlighem et al. (2017)

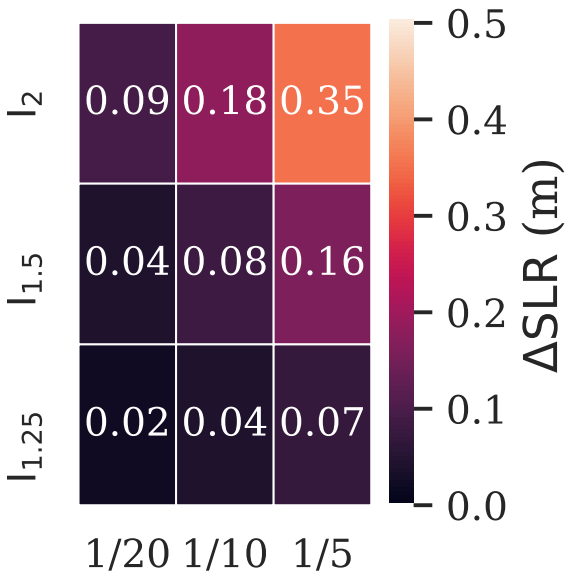

Fig. S26. Importance of intensity and frequency of extremes for the SMB-only case. Given is the projected sea-level rise contribution in year 2300 for the SMB-only case, for each extreme scenario, subtracted by the sea-level rise scenario without extremes (Miroc5) in 2300 (see also Table 2).

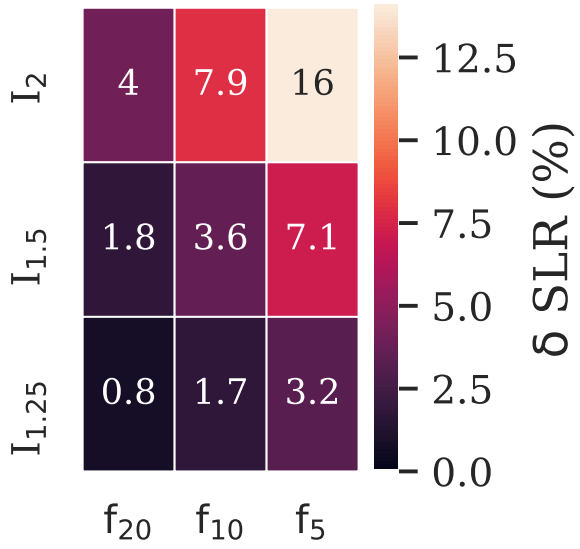

Fig. S27. Relative importance of intensity and frequency of extremes for the SMB only simulation. Given is the relative increase of the projected sea-level rise contribution in year 2300 of each extreme scenario to the scenario without extremes(MIROC5) for the SMB only case.

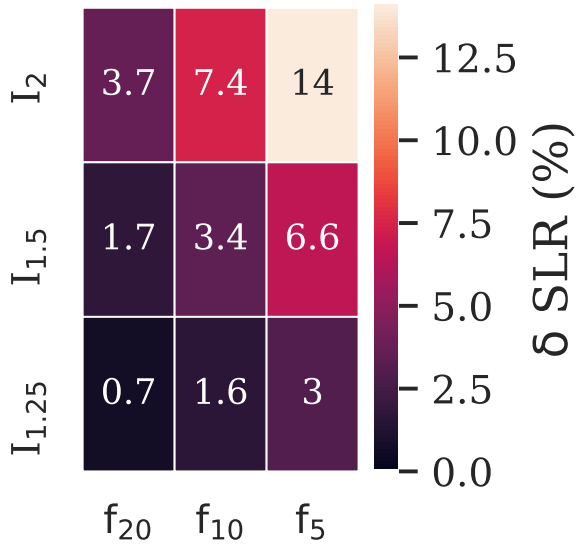

Fig. S28. Relative importance of intensity and frequency of extremes for the full dynamic simulation. Given is the relative increase of the projected sea-level rise contribution in year 2300 of each extreme scenario to the scenario without extremes(MIROC5) for the full dynamic simulations.

References

Delhasse, A., Fettweis, X., Kittel, C., Amory, C., and Agosta, C.: Brief communication: Impact of the recent atmospheric circulation change in summer on the future surface mass balance of the Greenland Ice Sheet, Cryosphere, 12, 3409–3418, https://doi.org/10.5194/tc-12-3409-2018, 2018.

Joughin, I., Smith, B. E., and Howat, I. M.: A complete map of Greenland ice velocity derived from satellite data collected over 20 years, Journal of Glaciology, 64, 1–11, https://doi.org/10.1017/jog.2017.73, 2018.

Morlighem, M., Williams, C. N., Rignot, E., An, L., Arndt, J. E., Bamber, J. L., Catania, G., Chauché, N., Dowdeswell, J. A., Dorschel, B., Fenty, I., Hogan, K., Howat, I., Hubbard, A., Jakobsson, M., Jordan, T. M., Kjeldsen, K. K., Millan, R., Mayer, L., Mouginot, J., Noël, B. P., O'Cofaigh, C., Palmer, S., Rysgaard, S., Seroussi, H., Siegert, M. J., Slabon, P., Straneo, F., van den Broeke, M. R., Weinrebe, W., Wood, M., and Zinglersen, K. B.: BedMachine v3: Complete Bed Topography and Ocean Bathymetry Mapping of Greenland From Multibeam Echo Sounding Combined With Mass Conservation, https://doi.org/10.1002/2017GL074954, 2017.

Mouginot, J., Rignot, E., Bjørk, A. A., van den Broeke, M., Millan, R., Morlighem, M., Noël, B., Scheuchl, B., and Wood, M.: Forty-six years of Greenland Ice Sheet mass balance from 1972 to 2018, Proceedings of the National Academy of Sciences of the United States of America, 116, 9239–9244, https://doi.org/10.1073/pnas.1904242116, 2019.

Palmer, M. D., Harris, G. R., and Gregory, J. M.: Extending CMIP5 projections of global mean temperature change and sea level rise due to thermal expansion using a physically-based emulator, Environmental Research Letters, 13, https://doi.org/10.1088/1748-9326/aad2e4, 2018.